Region-specific control of liposome fusion using an open-space fluidic online mixing system

Huan Luo [a], Nahoko Kasai [b], Chenhan Peng [a], Hizuru Nakajima [a], Shungo Kato [a], Hulie Zeng [c,*], Katsumi Uchiyama [a], Sifeng Mao [a,*]

[a]*Department of Applied Chemistry, Graduate School of Urban Environmental Sciences, Tokyo Metropolitan University, 1-1 Minami-osawa, Hachioji-shi, Tokyo 192-0397, Japan.*

[b]*University Education Center, Tokyo Metropolitan University, 1-1 Minami-osawa, Hachioji-shi, Tokyo 192-0397, Japan*

[c]*School of Pharmacy, Fudan University, 826 Zhangheng Road, Shanghai 201203, China*

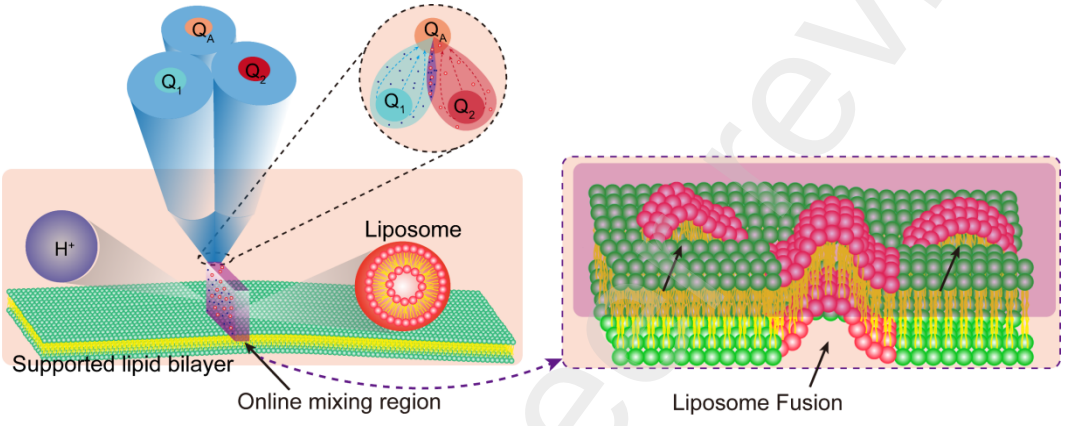

Region-specific control of liposome fusion using an open-space fluidic online mixing system

Huan Luo [a], Nahoko Kasai [b], Chenhan Peng [a], Hizuru Nakajima [a], Shungo Kato [a], Hulie Zeng [c,*], Katsumi Uchiyama [a], Sifeng Mao [a,*]

[a]*Department of Applied Chemistry, Graduate School of Urban Environmental Sciences, Tokyo Metropolitan University, 1-1 Minami-osawa, Hachioji-shi, Tokyo 192-0397, Japan.*

[b]*University Education Center, Tokyo Metropolitan University, 1-1 Minami-osawa, Hachioji-shi, Tokyo 192-0397, Japan*

[c]*School of Pharmacy, Fudan University, 826 Zhangheng Road, Shanghai 201203, China*

ARTICLE INFO

Keywords:
Membrane fusion
Region-specific control
Online mixing
Acidic condition

ABSTRACT

Lipid membrane fusion plays fundamental roles in both physiological and pathological processes, such as intracellular trafficking, tumor metastasis, and viral infection. The process is influenced by various environmental factors, particularly the pH condition. In this work, an open-space fluidic online mixing (OFM) system was employed for region-specific control of membrane fusion between small unilamellar vesicles (SUVs) and a supported lipid bilayer (SLB). The system manipulated processing fluids in an open space, providing the operational flexibility of precise positioning on the SLB. Under appropriate experimental conditions, the OFM system formed an online acidic mixing region benefiting from the hydrodynamic flow confinement, whose acidic condition locally aggregated the SUVs and further triggered the fusion of the SUVs into the SLB. The results indicate that the system has the capacity to control membrane fusion between SUVs and a SLB in a specific region. Moreover, this system is expected to control membrane fusion *in situ* at a single-cell level, since the created online mixing region at micrometers scale matches the size of a single cell. This OFM system offers an alternative tool for the region-specific control of membrane fusion, which benefits the fundamental understanding of the mechanisms and dynamics of membrane fusion, and furtherly advances the regulation of cellular processes with a high precision.

1. Introduction

Lipid membrane fusion is one of the most fundamental processes in organisms, whereby two separate lipid membranes merge into a single continuous bilayer, joining their membrane lipids and mixing their luminal contents. Lipid membrane fusion can occur between various vesicles and membrane structures, playing fundamental roles in numerous physiological, pathological, and technological processes, such as intracellular trafficking, neurotransmitter release, tumor metastasis, viral infection, and liposomal drug delivery (Cui et al., 2022; Meng et al., 2021; Jiang et al., 2024). Therefore, understanding membrane fusion events is essential for elucidating fundamental biological mechanisms and developing advanced biotechnological applications. The efficiency and regulation of lipid membrane fusion are influenced by a variety of factors, such as lipid composition, protein machinery, cellular signaling, and environmental conditions (Jumeaux et al., 2024; Duan et al., 2024; Das et al., 2020). Among these factors, pH, as one of the most important biochemical parameters in cellular environments, has attracted much attention. An acidic microenvironment is known to promote exosome traffic and uptake via the fusion pathway (Parolini et al., 2009; Milane et al., 2015). And recent research indicates that a low pH condition is a major determinant for viral fusion (Kreutzberger et al., 2022; Schowalter et al., 2009). These studies have yielded important insights into the mechanisms and regulation of membrane fusion influenced by pH, but they overlook the fusion efficiency and outcomes between local regions and that between individual cells.

Lipid membrane fusion that occurs either in a local specific area or within a single cell could offer more crucial information of fusion mechanisms, and that might allow a more precise regulation of cellular processes and targeted therapies with minimized side effects. This membrane fusion is highly dependent on changes in local conditions, particularly the aforementioned pH condition. Some techniques and approaches have been proposed to control the local pH. For instance, electrochemical methods had been used to generate a flux of protons in a controlled and quantifiable attempt to adjust the local pH in the vicinity of electrodes (Henckel et al., 2020; Zhang et al., 2020; Read et al., 2014).

*Corresponding author
E-mail address:maosifeng@tmu.ac.jp (S. Mao); zenghulie@fudan.edu.cn (H. Zeng)

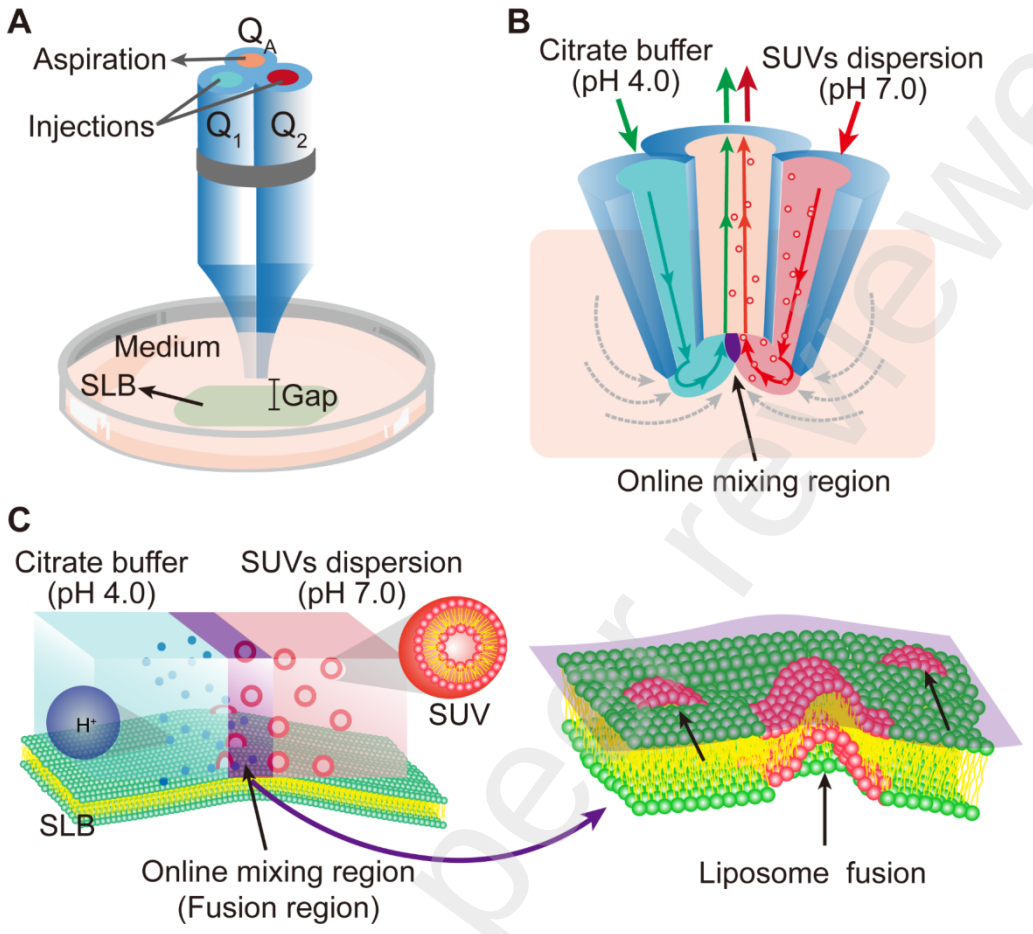

Fig. 1. The illustration for the OFM system to create the online mixing region with low pH for triggering the fusion of the SUVs with the SLB. (A) The structure of the OFM probe. (B) The formation of a laminar flow layers and an online mixing region. (C) The online mixing of the acidic buffer solution and the SUVs dispersion, and the fusion between the SUVs and the SLB at the online mixing region.

However, such methods are usually restricted by solvents and electrode materials and may introduce ions affecting lipid membrane fusion. Microfluidics has also been employed to create a pH gradient within the networks of the sealed microchannels and chambers (Jia et al., 2020; Yang et al., 2024; Rosella et al., 2021). Such devices have offered good platforms for studying local membrane fusion, but samples must be either passed through the channels or fixed in the designated positions, which potentially disrupted the whole-part relations, leading to the misinterpretation of local behaviors. Hence, studying local membrane fusion *in situ* has remained challenging.

In this work, an open-space fluidic online mixing (OFM) system was developed to control liposome fusion in a specific local region. This system controlled and manipulated fluids in an open space rather than within enclosed channels, which enabled the flexible operations of precise positioning on the target membranes. The OFM probe consisted of two injection apertures and one aspiration aperture. The injection flows formed laminar layers underneath the OFM probe by hydrodynamic flow confinement (Brimmo, et al., 2019), and the two layers mutually diffused to generate an online mixing region serving as working region (Mao et al., 2016; Zhang et al., 2018; Lin et al., 2019; Nishitani et al., 2022; Lin et al., 2022). The injection flows of the acidic buffer solution and the neutral small unilamellar vesicles (SUVs) dispersion created an online mixing region with low pH positioned on the surface of the SLB, where the acidic conditions locally triggered the SUVs fuse into the SLB (Fig. 1). In this way, the lipid membrane fusion of SUVs was controlled in the local online mixing region. Moreover, because the created online mixing region in several micrometers range could match the size of a single cell, SUVs could mimic exosomes or envelope viruses owe to the similarities of vesicle structure formed by a single phospholipid bilayer, and the SLB could mimic cell membranes due to its mechanical stability and lipid fluidity (Li et al., 2021; Jackman 2020), this system holds great potential for controlling membrane fusion of various vesicles and a single cell or even a subcellular compartment.

2. Materials and Methods

2.1 Materials and apparatus

1,2-dioleoyl-sn-glycero-3-phosphocholine (DOPC), 1,2-dioleoyl-sn-glycero-3-succinate (DGS), 1,2-dioleoyl-sn-glycero-3-phosphoethanolamine-N-(7-nitro-2-1,3-benzoxadiazol-4-yl) (ammonium salt) (NBD-PE), and 1,2-dioleoyl-sn-glycero-3-phosphoethanolamine-N-(lissamine rhodamine B sulfonyl) (ammonium salt) (Rhod-PE) were purchased from Avanti Polar Lipids, Inc. (USA) (Fig. S1, S2). pHrodo™ Green Dextran were purchased from Thermo Fisher Scientific, Inc. (USA). Aqueous solutions were prepared with ultrapure water (18.2 MΩ·cm^{-1}, 25 °C). Glass capillary tubes (0.6 mm × 1.0 mm) (MC-06, Nippon Rikagaku Kikai Co., Ltd. Japan); Fused silica inertness tubing (0.25 mm × 0.32 mm) (GL Sciences, Inc., Japan); PEEK tubes (0.5 mm × 1/16 inch) (Lab-system Co., Ltd., Japan); Syringes (1 mL) (Trajan Scientific and Medical Pty, Ltd., Australia); Syringe pumps (YMC Co., Ltd., Japan); a heat puller (PB-7) (NARISHIGE, Japan); a hand extruder (Genizer, LLC, U.S.A.).The flow layers and fusion results were observed using an inverted microscope and a total internal reflection fluorescence (TIRF) microscope (both supplied by the Olympus Co., Japan).

2.2 Preparation of SUVs

The thin-film hydration method was used to prepare the SUVs (Shah et al., 2020). Briefly, DGS and Rhod-PE (1 mol%) dissolved in chloroform was placed in a glass micro test tube. Chloroform was then evaporated using a rotary vacuum evaporator under a flow of argon gas until thin films had formed at the bottom. The solution was further dried in a vacuum desiccator overnight to ensure the complete removal of chloroform. Films were subsequently hydrated by PBS (0.1 M, pH 7.0), and were agitated for 30 seconds using a vortex mixer. The SUVs were finally dispersed by five freeze-thawing cycles, and the suspension was extruded with a 200 nm polycarbonate membrane filter for 11 times.

2.3 Preparation of the SLB

SLBs were prepared via the self-spreading method (Rädler et al., 1995) on the glass bottom. The glass bottom was washed by sonicating in the solution of 10 M NaOH, 1 M HCl in 70% ethanol and deionized water for 30 min each, followed by etching with an additional piranha solution (1:3 hydrogen peroxide to sulfuric acid) for 8 min. After that, it was rinsed exhaustively with deionized water, and was dried under nitrogen gas. One drop of the liposome suspension (DOPC with 1 mol% NBD-PE) was applied onto the cleaned glass bottom and allowed to dry under ambient conditions. After evaporation, a lipid lump was left on the glass, which was then immersed by a large volume of PBS (0.1 M, pH 7.0). The lipid bilayers spontaneously spread from the lipid lump on the glass at 37 ℃.

2.4 Fabrication and assembly of the OFM system

The OFM probe consists of two injection apertures and one aspiration aperture arranged a triangular shape, which was fabricated using a capillary heating-stretching technique (Fig. S3). Three glass capillary tubes were bundled together integrally and fixed on the heat puller. After heating, the glass tubes were pulled and subsequently cut into two separated portions to obtain two OFM probes. The cut plane of an OFM probe was polished to obtain a level and smooth surface using a progression of sandpapers (from 2000 to 10,000-grit). The probe nozzles were observed using a microscope. It was suggested that the inner diameter decreased with the increasing stretch length (Fig. S4). The OFM probe was then assembled to an injection/aspiration system and an XYZ stage (Fig. S5). The injection flow rates (Q_I) and the aspiration flow rate (Q_A) were properly adjusted by the syringe pumps, and the OFM probe was adjusted to a position parallel to the SLB with a certain gap by the XYZ stage.

3. Results and discussion

3.1 Mixing region width control

The injection flows were hydrodynamically confined entirely to form the laminar flow layers and generate the required online mixing region when the geometrical parameters and flow rates were properly adjusted. Therefore, the dominant system parameters, including flow-rate ratio ($Q = Q_A / Q_I$), gap, and OFM probe nozzles inner diameter, were investigated. To investigate the parameters, the fluorescein sodium and rhodamine B solution served as injections in order to visualize the laminar flow layers. The flow-rate ratio ($Q = Q_A / Q_I$) was firstly evaluated, which was adjusted by varying Q_I, while keeping Q_A constant at 200 μL·h^{-1}. It was illustrated that under a lower Q, the hydrodynamic force was not enough to completely confine the injection flows, resulting in a severe leakage in to the medium, as the Q increased to 20 and more, the hydrodynamic force could well confine the injection flows to from the laminar flow layers (Fig. S6).

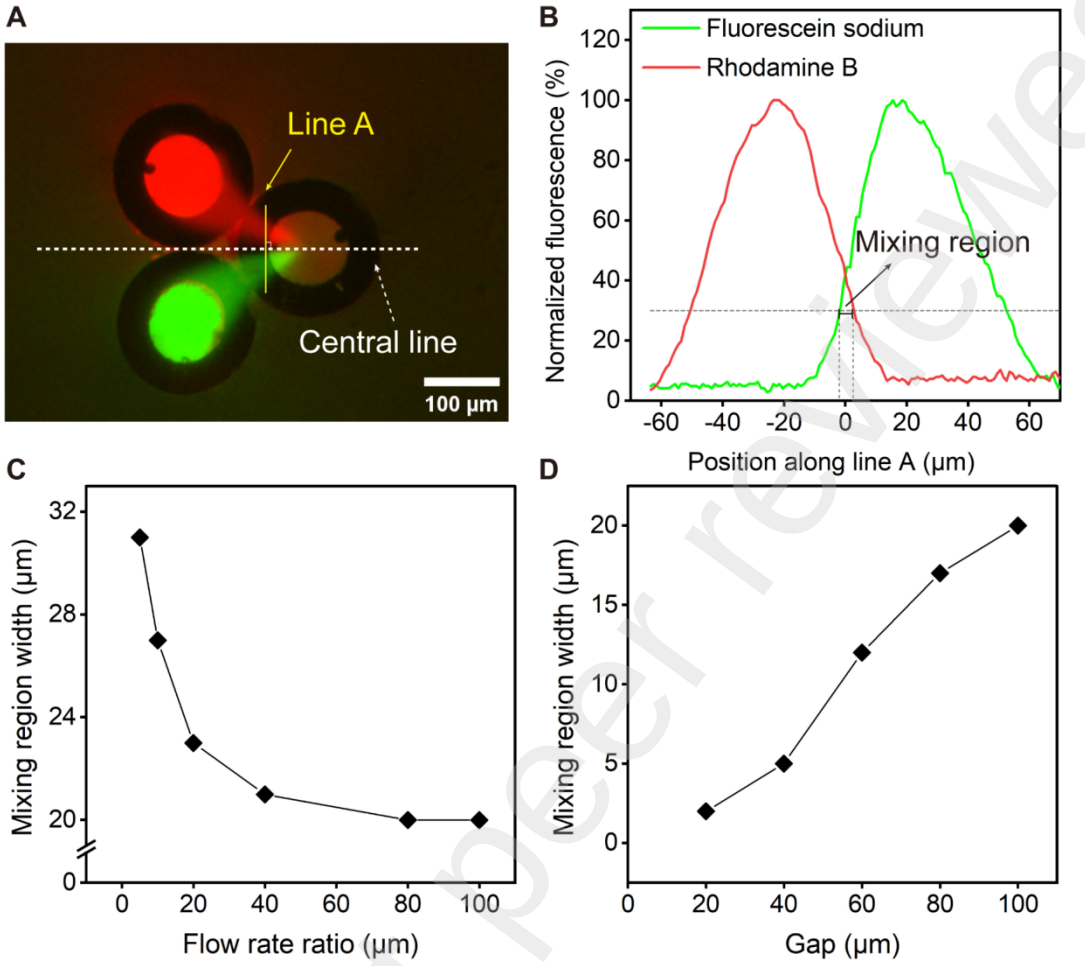

Fig. 2. (A) Bottom view of the OFM probe. (B) Normalized fluorescence intensity profile along "Line A" (I.D, 95 μm, Q_I = 5 μL·h^{-1}, Q_A = 200 μL·h^{-1}, Gap = 40 μm). (C) Mixing region widths under different flow rate ratio (I.D, 95 μm, Q_A = 200 μL·h^{-1}, Gap = 100 μm). (D) Mixing region widths under different gap values. (I.D, 95 μm, Q_I = 5 μL·h^{-1}, Q_A = 200 μL·h^{-1}).

The mixing region width was measured by "Image J" software. As shown in Fig. 2A, profiles of the fluorescence intensity were plotted along "Line A" (the solid line), which was perpendicular to the geometrical central line (the dotted line) of the probe nozzles. The intersection point was defined as 0 at the x axis, and the overlapping region of the plot profile of the fluorescence of rhodamine B and fluorescein sodium was considered as the mixing region (Fig. 2B). The boundary of the mixing region was defined by a normalized fluorescence intensity of 30% (three times larger than the noise intensity to eliminate the interference signals). The results indicated that the mixing region width decreased and reached a plateau as the Q increased (Fig. 2C), suggesting that adjusting Q within the range of 20 to 100 was appropriate. The Q was adjusted as 40 to furtherly investigate the influence of gap on mixing region width. The laminar flow layers under different gaps were observed, which showed that the injected flows were not fully confined when the gaps were equal to or less than 10 μm, while with a larger gap, the injected flows were confined and formed the laminar layers (Fig. S7). The mixing region widths were measured, which indicated that the width increased as the gap increased in the range of 20 μm to 100 μm (Fig. 2D). In addition, the influence of the inner diameters of the probe nozzles was also evaluated. It was demonstrated that the mixing region width increased as the inner diameter increased. (Fig. S8). The probe nozzles with an inner diameter of 95 μm (± 5 μm) was employed for the experiments.

According to the above results, it was confirmed that the variation of Q, in conjunction with the gap and nozzle inner diameter, can be used to control the width of the online mixing region.

3.2 Local mixing region with low pH

Acidic citrate buffer solutions (100 mM) and neutral NaCl (150 mM) solution were employed as the injections. pHrodo™ Green Dextran (10 μg·mL^{-1}) was added to both injections as the fluorescent pH indicator, whose fluorescence

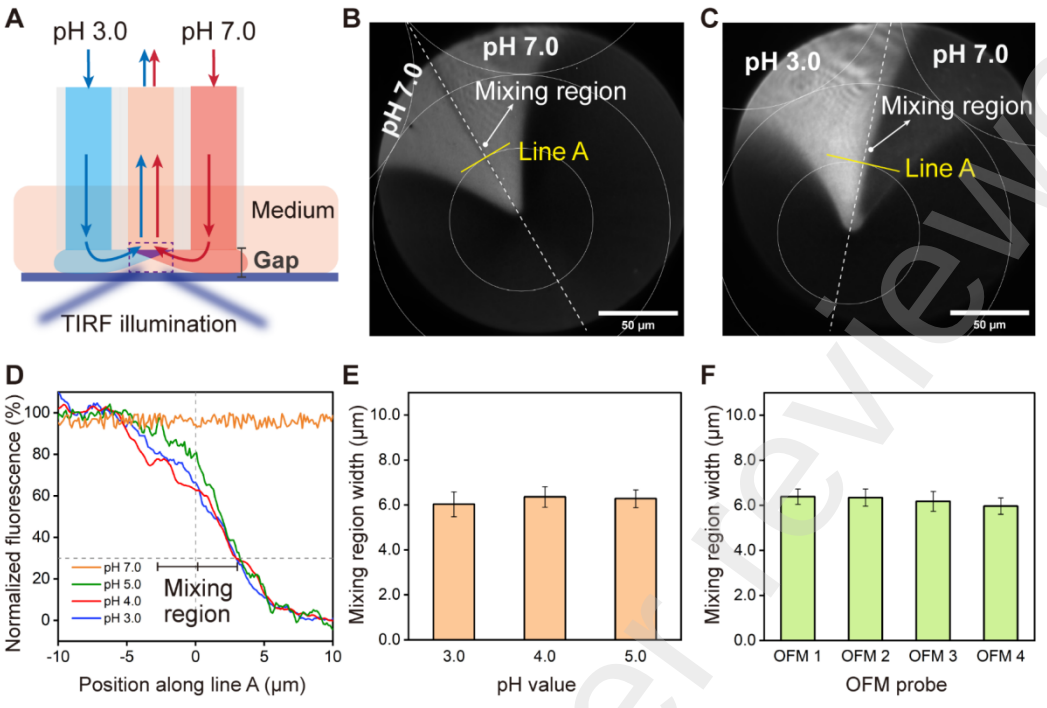

Fig. 3. The OFM system was employed to create a mixing region with low pH value. (A) An illustration of the manipulation of the OFM system. (B)-(C) TIRF images of the flow layers. The white circles outline the OFM probe nozzles, the mixing region was positioned in the middle area along the geometry central line. (D) Normalized fluorescence intensity profile along "Line A" for one injection at pH 7.0 and the other injection at pH 3.0, 4.0, 5.0, or 7.0. (E) Mixing region widths for one injection one injection at pH 7.0 and the other injection at pH 3.0, 4.0, or 5.0. (F) Mixing region widths obtained via four OFM probes under consistent parameters and experimental conditions.

emission increases in intensity with increasing acidity (Fig. S9). A TIRF microscope was utilized to observe the laminar flow layers on the glass bottom (Fig. 3A). It was observed that when the injection flows were both neutral, the two flow layers almost merge into one flow layer with uniform fluorescence intensity, which indicated that the mixing region had almost same fluorescence intensity, i.e., the almost same pH (Fig. 3B). However, when the injections were at pH 3.0 and 7.0, the flow layer with higher fluorescence intensity was larger than the dimmer one, which indicated that the mixing region had higher fluorescence intensity, i.e., the lower pH (Fig. 3C). The acidic mixing region widths were determined using the plot profiles of the fluorescence intensity along "Line A" (Fig. 3D). The boundaries of the mixing region were also defined with a normalized fluorescence intensity of 30%. The results demonstrated that the mixing region widths were almost the same even though the acidic flow had different pH, and the average width of the mixing region was 6.2 μm with good stability (RSD = ± 0.47%) (Fig. 3E), which possibly due to the similar diffusion coefficients of the buffering agents, The good reproducibility of the mixing region width was also confirmed by using four different OFM probes for the experiments under consistent experimental conditions. (Fig. S10, Fig. 3F)

3.3 Lipid membrane fusion in an acidic environment

The SLB spread on the glass bottom was examined by fluorescence recovery after photobleaching (FRAP) to evaluate the lipid fluidity. Fig. S11 showed the representative time courses of the fluorescence recovery. After 10 min, the fluorescence intensity of the bleach area had recovered by approximately 80%, which suggested the reasonable fluidity of the prepared SLB (Han et al., 2010). SUVs dispersion (pH 7.0) was added into SLBs with surrounding medium at either pH 7.0 or pH 4.0 for 30 min. After that, in the medium at pH 7.0, the fluorescence intensity derived from NBD-PE in the SLB showed a decrease of 7%, and it was observed that a few fluorescent spots of SUVs were absorbed on the SLB, while more spots were scattered on the glass bottom outside the SLB (Fig. 4A-D). It was probably due to the electrostatic repulsion between the SUVs and the SLB under a neutral condition and the combination of the carboxylic acid groups of DGS in the SUVs and the hydroxyl groups on the glass. It implied that almost no fusion occurred at this condition, and the minor fluorescence decreases in the NBD-PE might arise from the slight variations of light source.

In the acidic medium (pH 4.0), the fluorescence intensity derived from NBD-PE decreased by 32%, and the uniform

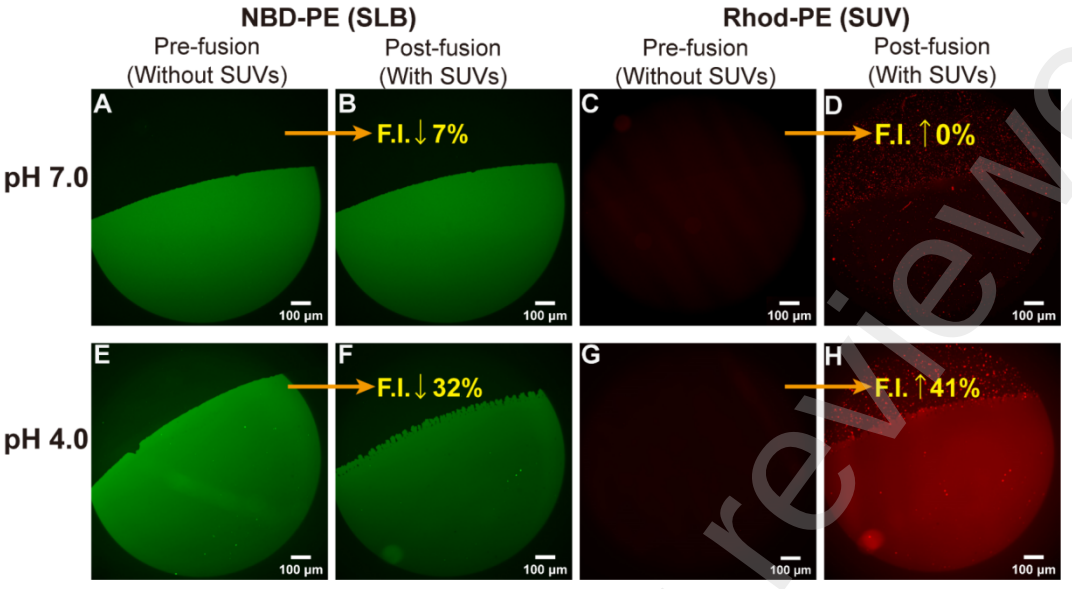

Fig. 4. The fusion between the SUVs and the SLB in either a neutral environment (pH 7.0) or an acidic environment (pH 4.0). The green fluorescence emitted by NBD-PE and the red fluorescence emitted by Rhod-PE (F.I.: Fluorescence intensity).

fluorescent area derived from Rhod-PE was observed and increased by 41% (Fig. 4E-H). The fluorescence intensity changes were attributed to the lipid fusion of the SUVs and the SLB. The fusion caused the SUVs lipids joining and rearrangement in the lipid bilayer, which not only led to a lower concentration of NBD-PE and a higher concentration of Rhod-PE in the fusion region, but also induced the Förster resonance energy transfer (FRET) effect between Rhod-PE (acceptor fluorophore) and NBD-PE (acceptor fluorophore) because they were simultaneously existed with the close distance in the fused SLB. As a consequence, the fluorescence intensity derived from Rhod-PE increased while that from NBD-PE decreased. The results indicated that the acidic condition was essential to trigger the lipid membrane fusion between SUVs and SLB, which was probably due to that the acidic condition facilitated the protonation of the carboxylic acid groups of DGS in SUVs, making SUVs become more hydrophilic, increasing their surface aggregation on the SLB, followed by fusion into the SLB (Drummond et al., 2000).

3.4 Lipid membrane fusion controlled by OFM system

The citrate buffer solution (0.1 M, pH 4.0) and SUVs dispersion in NaCl solution (150 mM, pH 7.0) were used as the injection flows. The neutral NaCl solution helped maintain SUVs integrity and prevented their aggregation (Drummond et al., 2000). SLB spread on the glass bottom with neutral surrounding medium, and the probe nozzles were immersed in the medium and located parallel to the glass with a certain gap. After the OFM system working for 600s, a noticeable dark area was observed on the bilayer in the online mixing region under NBD-PE excitation/emission wavelength compared with the pre-fusion state (Fig. 5A-1,2), and the red fluorescent signals derived from Rhod-PE simultaneously appeared at the same area (Fig. 5A-5,6). The results indicated that membrane fusion between the SUVs and the SLB had occurred in this specific region. The fusion induced the SUVs lipids inserting into the SLB, thereby would cause either or both the FRET effect or/and the concentration changes of Rhod-PE and NBD-PE in this area. Additionally, it was observed that the fluorescence intensity derived from Rhod-PE in the mixing region was stronger than that in the surrounding areas (Fig. 5A-6), which implied a high concentration of SUV particles in the online mixing region. This was the result of that the acidic condition of the mixing region facilitated surface aggregation of SUVs on the SLB (Drummond et al., 2000). The aggregation was the first step of the fusion of SUVs with the SLB, and the fusion states were illustrated in Fig. 5B (Chernomordik et al., 2008). The Rhod-PE fused into the bilayer and diffused outwards from the mixing region towards the perimeters with the fluidity of the lipid bilayer, leading to the weaker intensity derived from Rhod-PE around the mixing region.

The fluorescence intensity of NBD-PE and Rhod-PE was monitored over time after removing the OFM probe. Here, the OFM working time of 600 s was equal to OFM removal time of 0 s. It was showed that the dark area in NBD-PE progressively disappeared, and the fluorescence intensity became uniform (Fig. 5A-2,3,4). The fluorescence intensity of NBD-PE in the circled area recovered to 67% after 900 s (Fig. 5C). The lower recovery rate indicated less lipid fluidity

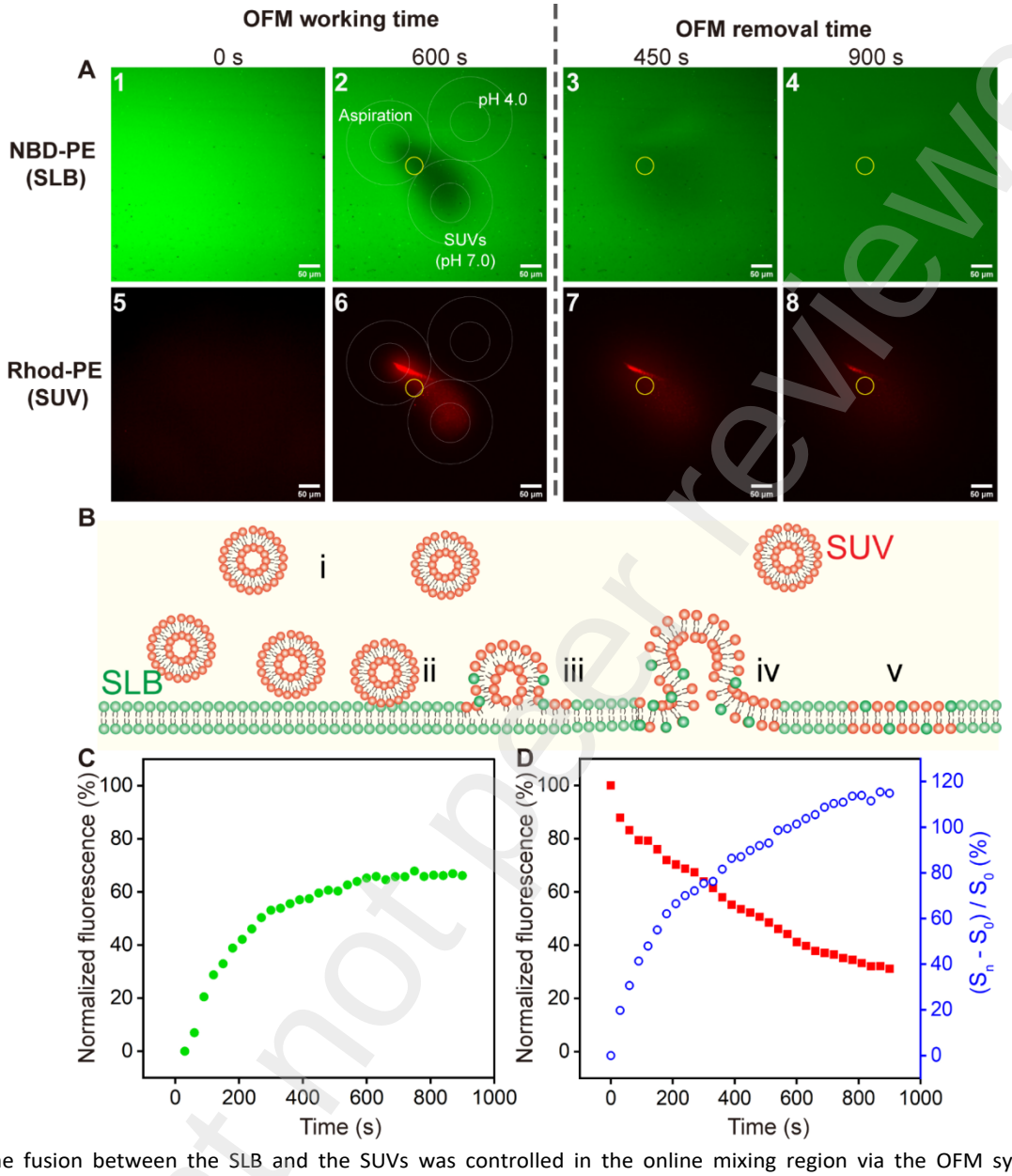

Fig. 5. The fusion between the SLB and the SUVs was controlled in the online mixing region via the OFM system. (A) Fluorescence images of different working times and removal times. (B) The various fusion states between the SUVs and the SLB. (i) Aggregation: the SUVs gathered and contacted the SLB; (ii) Docking: the SUVs and the SLB came into even closer contact; (iii) Hemifusion: the outer leaflets merged, but the inner leaflet remained separate; (iv) Fusion pore: the outer leaflets and the inner leaflet merged; (v) Full fusion: the two membranes completely merged into one continuous membrane. (C) The fluorescence intensity derived from NBD-PE at the circled area changed over time after removing the OFM probe. (D) The fluorescence intensity derived from Rhod-PE in the circled area (red square) and the fluorescent area size (blue open circle) changed over time after removing the OFM probe. (S_n: Fluorescent area size after removal of the OFM probe, S_0: Fluorescent area size when the removal time was 0 s.)

in the fused bilayer compared to the original SLB (Fig. S11). It was possibly due to the fact that some SUVs at hemifusion state existed during the fusion process, which acted as obstacles to the lateral diffusion of fused lipids. This result could also be considered as one piece of the evidences supporting the fusion-through-hemifusion pathway (Chernomordik et al., 2008). Moreover, a decrease in fluorescence intensity derived from Rhod-PE in the circled area (red squares in Fig. 5D) and an increase in the overall fluorescent area were observed (blue open circles in Fig. 5D). The fluorescent area size was obtained by transforming the fluorescence images into the fluorescence intensity contour maps and measuring

the area based on defining the boundary as 30% normalized fluorescence intensity (Fig. S12). The results demonstrated that the already merged Rhod-PE continually diffused laterally in the lipid bilayer, resulting a wilder distribution with a lower density.

Thus, according to the above results, the OFM system enabled to control lipid membrane fusion of SUVs into a SLB in a precisely positioned region. Additionally, it also offered a tool to examine the lipids lateral fluidity of SLBs.

4. Conclusion

A OFM system was proposed for region-specific control of membrane fusion between SUVs and SLB. The system manipulated and confined fluids in an open space, providing the operational flexibility of precise positioning on the target samples. Under the appropriate system parameters, it formed the laminar flow layers and generated a local mixing region with acidic pH at 6.2 μm in width. It furtherly employed to create an online mixing region with low pH for locally aggregating and triggering the fusion of SUVs into the SLB. Due to the single lipid bilayer structures of SUVs and SLBs, the system holds the potential for region-specific control of membrane fusion between various biological vesicles, different intracellular compartments, and cellular membranes. Additionally, it offers a potential tool for processing at a single-cell level owe to the mixing region with dimensions on the order of micrometers as working region. After fusion, the lipid lateral fluidity of the fused bilayer was confirmed according to the fluorescence recovery of NBD-PE and the fluorescence changes of Rhod-PE, which would offer a novel method to determine the lipid lateral diffusion in bilayers instead of FRAP assay. This study benefits the fundamental understanding and elucidation of the mechanisms and dynamics of membrane fusion in critical cellular processes, which is critical for the regulation of cellular processes with a high precision and for the development of targeted drug delivery and therapy. Additionally, the system offers a versatile tool in a wide range of research fields, because it could generate diverse online mixing regions with different sizes and properties to cater to various research purposes conditions by altering the experimental conditions, including the system parameters, injection solutions, and the number of nozzles.

CRediT authorship contribution statement

H. Luo: Writing – original draft, Methodology, Validation, Formal analysis, Data curation, Investigation. **N. Kasai**: Conceptualization, Methodology, Supervision, Funding acquisition, Project administration, Writing-review and editing. **C. Peng**: Validation, Formal analysis, Data curation. **H. Nakajima**: Funding acquisition, Supervision, Writing-review and editing. **S. Kato**: Supervision, Writing-review and editing. **H. Zeng:** Methodology, Supervision, Writing-review and editing. **K. Uchiyama**: Conceptualization, Methodology. **S. Mao**: Conceptualization, Methodology, Supervision, Project administration, Formal analysis, Writing-review and editing.

Declaration of competing interest

The authors declare that they have no known competing financial interests or personal relationships that could have appeared to influence the work reported in this paper.

Data availability

The data that has been used is confidential.

Acknowledgments

This study was supported by Tokyo Metropolitan Government Advanced Research (Grant Number R4-1), the Infectious Disease Research Project, JSPS KAKENHI (Grant Number 21K14653), and TMU strategic research fund of the faculty for internationalization promotion research fund.

Appendix A. Supplementary data

Supplementary data to this article can be found online.

References

Cui, L., Li, H., Xi, Y., Hu, Q., Liu, H., Fan, J., Xiang, Y., Zhang, X., Shui, W., Lai, Y., 2022. Mol Biomed. 2022, 3 (1), 29.

Meng, Q. F., Zhao, Y., Dong, C., Liu, L., Pan, Y., Lai, J., Liu, Z., Yu, G. T., Chen, X., Rao, L., 2021. Angew. Chem. Int. Ed. 60 (50), 26320-26326.

Jiang, S., Cai, G., Yang, Z., Shi, H., Zeng, H., Ye, Q., Hu, Z., Wang, Z., 2024. ACS Nano 18(18), 11753-11768.

Jumeaux, C., Spicer, C. D., Charchar, P., Howes, P. D., Holme, M. N., Ma, L., Rose, N. C., Nabarro, J., Fascione, M. A., Rashid, M. H., Yarovsky,

I., Stevens, M. M., 2024. Angew. Chem. Int. Ed. 63 (14), e202314786.

Duan, M., Gao, G., Lin, A., Mackey, E. J., Banfield, D. K., Merz, A. J., 2024. J. Cell Biol. 223(6), e202001034.

Das, D. K., Bulow, U., Diehl, W. E., Durham, N. D., Senjobe, F., Chandran, K., Luban, J., Munro, J. B., 2020. PLoS Biol. 18 (2), e3000626.

Parolini, I., Federici, C., Raggi, C., Lugini, L., Palleschi, S., De Milito, A., Coscia, C., Iessi, E., Logozzi, M.,Molinari, A., Colone, M., Tatti, M., Sargiacomo, M., Fais, S., 2009. J. Biol. Chem. 284 (49), 34211-22.

Milane, L., Singh, A., Mattheolabakis, G., Suresh, M., Amiji, M. M., 2015. J. Control Release 219, 278-294.

Kreutzberger, A. J. B., Sanyal, A., Saminathan, A., Bloyet, L. M., Stumpf, S., Liu, Z., Ojha, R., Patjas, M. T., Geneid, A., Scanavachi, G., Doyle, C. A., Somerville, E., Correia, R., Di Caprio, G., Toppila-Salmi, S., Makitie, A., Kiessling, V., Vapalahti, O., Whelan, S. P. J., Balistreri, G., Kirchhausen, T., 2022. Proc. Natl. Acad. Sci. 119 (38), e2209514119.

Schowalter, R. M.; Chang, A.; Robach, J. G.; Buchholz, U. J.; Dutch, R. E.,2009. J. Virol. 83 (3), 1511-1522.

Henckel, D. A., Counihan, M. J., Holmes, H. E., Chen, X., Nwabara, U. O., Verma, S., Rodríguez-López, J., Kenis, P. J. A., Gewirth, A. A., 2020. ACS Catalysis 11 (1), 255-263.

Zhang, F., Co, A. C., 2020. Angew. Chem. Int. Ed. 59 (4), 1674-1681.

Read, T. L.; Bitziou, E., Joseph, M. B., Macpherson, J. V., 2014. Anal. Chem. 86 (1), 367-371.

Jia, N. Rosella, E., Juere, E., Pouliot, R., Kleitz, F., Greener, J., 2020. Lab Chip 20 (6), 1066-1071.

Yang, Q., Zhou, X., Lou, B., Zheng, N., Chen, J., Yang, G., 2024. Acta Biomater. 179, 207-219.

Rosella, E., Jia, N., Mantovani, D., Greener, J., 2021. J. Mater. Sci. Technol. 63, 54-61.

Brimmo, A.T.; Menachery, A.; Qasaimeh, M. A., 2019. Lab Chip 19(24):4052-4063.

Mao, S., Sato, C., Suzuki, Y., Yang, J., Zeng, H., Nakajima, H., Yang, M., Lin, J. M., Uchiyama, K., 2016. Chemphyschem. 17 (20), 3155-3159.

Zhang, Y., Mao, S., Suzuki, Y., Tanaka, Y., Kawaguchi, M., Zhang, W., Zeng, H., Nakajima, H., Yang, M., Uchiyama, K., 2018. Chem. Commun. 54 (7), 719-722.

Lin, H., Mao, S., Zeng, H., Zhang, Y., Kawaguchi, M., Tanaka, Y., Lin, J. M., Uchiyama, K., 2019. Anal. Chem. 91 (11), 7346-7352.

Nishitani, Y., Kasai, N., Nakajima, H., Kato, S., Mao, S., Uchiyama, K., 2022. Chem. Commun. 58 (27), 4308-4311.

Lin, H., Kasai, N., Xu, N., Nakajima, H., Kato, S., Zeng, H., Lin, J. M., Mao, S., Uchiyama, K., 2022. Biosens. Bioelectron. 218, 114788.

Li, H., Gao, J., Cao, L., Xie, X., Fan, J., Wang, H., Wang, H. H., Nie, Z., 2021. Angew. Chem. Int. Ed. 60 (50), 26087-26095.

Jackman, J. A., Cho, N.-J., 2020. Langmuir 36 (6), 1387-1400.

Shah, S., Dhawan, V., Holm, R., Nagarsenker, M. S., Perrie, Y., 2020. Adv. Drug Deliv. Rev. 154, 102-122.

Rädler, J., Strey, H., Sackmann, E., 1995. Langmuir 11, 4539-4548.

Han, X., Achalkumar, A.S., Cheetham, M.R., Connell, S.D.A., Johnson, B.R.G., Bushby, R.J., Evans, S.D., 2010. ChemPhysChem. 11, 569-574.

Drummond, D. C.; Zignani, M.; Leroux, J. C., 2000. Prog. Lipid Res. 39 (5), 409-460.

Chernomordik, L. V., Kozlov, M. M., 2008. Nat. Struct. Mol. Biol. 15 (7), 675-683.